Astron. Astrophys. 176, 267–284 (1987)

ASTRONOMY
AND
ASTROPHYSICS

Rotational modulation and flares on RS CVn and BY Dra stars

III. IUE observations of V711 Tau (=HR 1099), II Peg, and AR Lac★

M. Rodonò[1], P.B. Byrne[2], J.E. Neff[3], J.L. Linsky[3]★★, T. Simon[4], C.J. Butler[2], S. Catalano[1], G. Cutispoto[1], J.G. Doyle[2], A.D. Andrews[2], and D.M. Gibson[5]

[1] Istituto di Astronomia, Università degli Studi, Viale A. Doria 6, I-95125 Catania, Italy
[2] Armagh Observatory, Armagh BT61 9DG, Northern Ireland
[3] Joint Institute for Laboratory Astrophysics, University of Colorado, Boulder, CO 80309, USA
[4] Institute for Astronomy, University of Hawaii, 2680 Woodlawn Dr., Honolulu, HI 96822, USA
[5] Department of Physics and Astronomy, New Mexico Institute of Mining and Technology, Socorro, NM 87801, USA

Received July 23, accepted September 11, 1986

Summary. We present observations of three RS CVn stars, which were obtained over the stellar rotation cycles with the *IUE* satellite. Emission lines from high-temperature transition regions and chromospheres analogous to those observed in the solar spectrum were observed. However, the stellar line surface fluxes are hundreds of times the solar values.

The only visible component of II Peg and both components of V711 Tau and AR Lac appear to be chromospherically active. For the latter systems, the Mg II line surface flux from the G-type star is higher than that from the K subgiant, which dominates the observed UV line flux. Moreover, evidence of long-term ultraviolet variability is presented for AR Lac.

The emission line fluxes for II Peg and, marginally, for the other two systems were observed to vary in anti-phase with the optical variations at the time of our IUE observations. By comparing the results of two-spot models from Paper I with the variation of UV line flux, we find evidence of a close spatial correlation between spot and plage-like features. We interpret these correlations in terms of large spot areas in the stellar photospheres with overlying magnetic loops, which form plages in the outer atmosphere. Some evidence is presented for non-thermal gas motions, which might be associated with the most active regions of the stars.

Key words: stellar atmospheres – late-type stars – RS CVn binaries – IUE spectra – surface activity – starspots and plages

1. Introduction

The RS CVn-type stars are close binaries that share a number of common features (Hall, 1976). Their periods lie in the range from ~0.5 to 20 days and they generally are composed of a K-type subgiant or giant with a main sequence or subgiant companion, typically of spectral type G. Their optical spectra show strong emission reversals in the Ca II H and K lines and sometimes in the hydrogen Balmer lines (Bopp, 1983). Periodic light variations, which are wavelike in character and have a period nearly equal to the orbital period (Hall, 1981; Rodonò, 1981; Catalano, 1983), are also seen. Long duration radio flares are also reported in some cases (Feldman et al., 1978; Catalano, 1986, and references therein).

The prototype of RS CVn-type systems, RS CVn itself, was discovered by Catalano and Rodonò (1967) to be optically variable. Since then it has been realized that the wavelike photometric variations and other phenomena found in the RS CVn binaries can be explained by large-scale photospheric spots, similar in nature to sunspots, which are distributed unevenly over the stellar surface (Eaton and Hall, 1979). Stellar magnetic fields associated with spots probably serve to heat chromospheres, transition regions, and coronae, which are detected predominantly by their far UV and X-ray emissions. These magnetic fields arise via dynamo effects from the interaction of rapid rotation and deep convection. Many reviews discuss the RS CVn stars from both observational and theoretical points of view. The most recent ones illustrate the various facets of stellar activity in RS CVn and related objects (Hall, 1981; Rodonò, 1981, 1983; Belvedere, 1983; Bopp, 1983; Catalano, 1983, 1986; Charles, 1983; Linsky, 1984).

Ultraviolet studies can make fundamental contributions to our understanding of this class of objects, because many of the most important diagnostic emissions for stellar chromospheres and transition regions are located in the far ultraviolet. Owing to its sensitivity, the *International Ultraviolet Explorer* (*IUE*) satellite has made careful study of the RS CVn stars in the UV possible. The first UV studies of RS CVn's were made with the *Copernicus* satellite. Weiler et al. (1978) observed V711 Tau (=HR 1099) and UX Ari in Mg II h and k and Ly α and found evidence for possible mass motions in their atmospheres. *Copernicus* was relatively insensitive compared to *IUE*, so the observations were limited in phase resolution and to bright spectral

Send offprint requests to: M. Rodonò

★ Based on observations collected with IUE at the ESA Satellite Tracking Station, Villafranca (Spain) and at NASA Goddard Space Flight Center, Greenbelt, MD, USA

★★ Staff Member, Quantum Physics Division, National Bureau of Standards

features. Early studies of RS CVn systems using *IUE* include those of V711 Tau and λ And by Linsky et al. (1978) and of V711 Tau and UX Ari by Simon and Linsky (1980). Their observations showed a number of chromospheric and transition region emission lines that implied stellar surface fluxes of up to several hundred times the typical solar values. Simon and Linsky (1980) found evidence for line strength variations in V711 Tau, but they were unable to detect any correlation with orbital (and therefore rotational) phase. Marginal evidence of rotationally modulated UV emission-line flux was obtained by Blanco et al. (1979) for the solar-type star HD 206860, by Rodonò et al. (1980) for II Peg, and by Baliunas and Dupree (1982) for λ And. These observations showed that UV emission lines were brighter close to the time of photometric minima (i.e., near maximum spot coverage) and implied, by analogy with the Sun, that plages overlay spots.

Here we present *IUE* observations of three RS CVn binaries, which were aimed at uniform coverage with respect to orbital phase over more than one cycle in each case, in order to examine changes in chromospheric and transition region structure accompanying the spot phenomenon. Preliminary results have been presented at several meetings (Andrews et al., 1983; Byrne et al., 1982, 1984; Linsky, 1983, 1984; Marstad et al., 1982; Rodonò, 1983, 1984, 1986).

2. Observations

Joint ground-based and *IUE* observations of the RS CVn systems V711 Tau (= HR 1099 = HD 22468), II Peg (= HD 224085), and AR Lac (= HD 210334) were undertaken during the interval 1–7 October, 1981. The principal characteristics of the program stars and of their orbits are given in Table 1.

The results of the ground-based campaign form the subject matter of a previous paper in this series (Rodonò et al., 1986, Paper I). The maps in Figure 1 summarize the principal results of Paper I concerning spot modelling of the program stars' light curves. The purpose of these maps is to show any spatial correlation between spot and plage location, the latter determined from the *IUE* data discussed below. The *IUE* data were received at the ESA ground station at Vilspa (Madrid) and at NASA's Goddard Space Flight Center. Observations were spaced in time so as to provide nearly uniform photometric phase coverage.

Table 1. Characteristics of program stars and their orbits

Variable Name	V711 Tau		Ref.	II Peg	Ref.	AR Lac		Ref.
Catalogue No.	HD 22468 SAO 111291			HD 224085 SAO 91578		HD 210334 SAO 51684		
V(mag)	5.85[a]		1	7.44[a]	1	6.15[a]		1
V-R(mag)	+0.81[a]		1	+0.89[a]	1	+0.75[a]		1
d(pc)	31		2	30	2	40		3
Spectral Types	K1 IV	G5 V	4	K2 IV	5	G2 IV-V	K0 IV	6
M/M⊙	1.4 ±0.2	1.1 ±0.2	4	f(m)=0.035	5	1.35	1.35	3
R/R⊙	3.9 ±0.2	1.3 ±0.2	4	2.8 (for i=90°)	5	1.52	2.77	7
L/L(tot) (V-band)	0.65 ±0.01	0.35 ±0.01	1	1.0 ±0.01	1	0.41	0.59	3
Veq(km s^{-1})	70 ± 4	24 ± 4	4	24 ± 2[b]	5	39	72	3
a sin i (10^6 km)	1.93 ±0.2	2.41 ±0.2	4	3.40 ±0.11	5	3.17	3.15	8
K (km s^{-1})	49.4 ±0.5	61.7 ±0.6	4	36.8 ± 1.2	5	116.1	115.6	8
γ (km s^{-1})	-15.0 ±0.3		4	-18.1 ±0.9	5	-33.7		8
To (HJD) orb.:	2,442,766.080		4	2,442,021.7264	5	2,444,977.0216		1
phot.:	2,442,766.069		1	--		--		
P(days) orb:	2.83774		4	6.724464	1	1.983170		1
phot.:	2.83782		1	--		--		
i (degrees)	33		4	90 (assumed)	9	87±2		3
e	0.014 ±0.009		4	0.033 ±0.035	5	0.041		3

References. 1: Rodono' et al., 1986 (Paper I); 2: Jenkins, 1963; 3: Chambliss, 1976; 4: Fekel, 1983; 5: Vogt, 1981; 6: Naftilan and Drake, 1977; 7: Walter et al., 1983; 8: Sanford, 1951; 9: Highly uncertain value; Poe and Eaton (1985) assume i = 60°.

Notes: a = Joint photometry of system components; b = Computed from v sin i given by Vogt (1981) and assuming i = 60°.

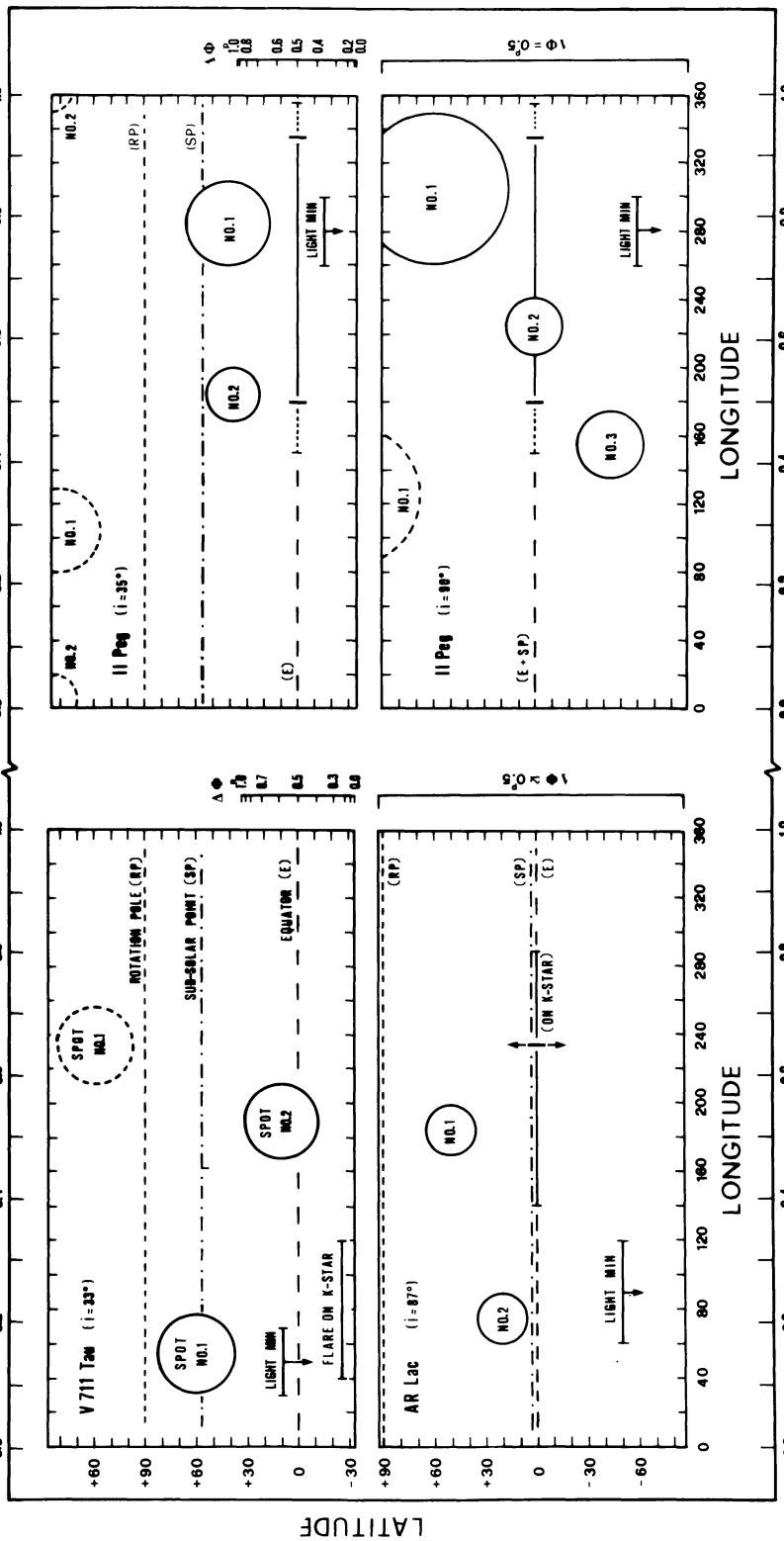

Fig. 1. Mercator-type maps of the stellar surface with "spots" (*circles*) from two-spot models in Paper I. *Continuous* and *broken circles* refer to the spot position at stellar meridian and 180-degree apart, respectively. Zero phase and zero longitude are reckoned from the orbital ephemerides in Table 1, corresponding to superior conjunction (larger star in front) and to the stellar meridian at that epoch, respectively. The scales to the right of each panel indicate the phase interval ($\Delta\phi$) during which a point-like feature – located at the latitude given by the corresponding scale on the left – is on the hemisphere facing the observer. Latitudes north of those corresponding to $\Delta\phi = 1.0$ are always visible. For AR Lac ($i = 87°$) all parts of its surface are visible for about one-half of the rotation period ($\Delta\phi \sim 0.5$), except for a circular area within 3° of the north and south poles, which are always and never visible, respectively. The *continuous horizontal lines* indicate the phase interval during which line flux enhancement is observed. *Dotted lines* indicate the phase interval of line increase to peak flux (*heavy vertical bar*) or decay to minimum flux

Table 2. Log of *IUE* spectra

Star	JD (2,444,000.+) (a)	Exposure Time (mins)	Image No.- Dispersion (b)	Orbital Phase (a)
V711 Tau	879.92981	60.0	SWP15153-LO	0.906
	879.95871	15.0	LWR11660-HI	0.916
	880.38451	15.0	LWR11665-HI	0.066
	880.41751	45.0	SWP15158-LO	0.078
	880.71696 (c)	35.0	SWP15161-LO	0.183
	880.77461 (c)	15.0	LWR11668-HI	0.204
	880.94919 (c)	15.0	LWR11670-HI	0.265
	881.00578 (c)	120.0	SWP15163-HI	0.285
	881.05674 (c)	15.0	LWR11671-HI	0.303
	881.07593 (c)	15.0	SWP15164-LO	0.310
	881.39901	15.0	LWR11674-HI	0.424
	881.41510	25.0	SWP15167-LO	0.429
	881.77718	15.0	LWR11679-HI	0.557
	881.79987	35.0	SWP15170-LO	0.565
	882.10532	35.0	SWP15173-LO	0.673
	882.12540	15.0	LWR11683-HI	0.680
	883.04857	12.0	LWR11691-HI	0.005
	883.07226	28.0	SWP15183-LO	0.011
	884.95575	15.0	LWR11715-HI	0.677
	884.97500	30.0	SWP15197-LO	0.684
II Peg	879.14563	25.0	LWR11652-HI	0.929
	879.19184	100.0	SWP15147-LO	0.936
	879.63698	25.0	LWR11655-HI	0.002
	879.68108	80.0	SWP15151-LO	0.009
	880.59555	35.0	LWR11667-HI	0.145
	880.66328	80.0	SWP15160-LO	0.151
	881.26462	35.0	LWR11673-HI	0.244
	881.31566	100.0	SWP15166-LO	0.252
	881.86902	45.0	LWR11680-HI	0.334
	881.91652	80.0	SWP15171-LO	0.341
	882.20908	80.0	SWP15174-LO	0.384
	882.25112	35.0	LWR11684-HI	0.391
	882.95268	30.0	LWR11690-HI	0.495
	882.98564	50.0	SWP15182-LO	0.500
	884.86952	35.0	LWR11714-HI	0.780
	884.89837	40.0	SWP15196-LO	0.784
AR Lac	67.48659	100.0	SWP 5777-LO	0.373
	67.53520	30.0	LWR 5023-HI	0.398
	70.46278	100.0	SWP 5810-LO	0.874
	70.51895	50.0	LWR 5059-HI	0.902
	524.16420	115.0	SWP10329-LO	0.650
	524.22473	50.0	LWR 9003-HI	0.680
	525.39175	50.0	LWR 9010-HI	0.269
	525.33601	97.0	SWP10352-LO	0.241
	880.11911	30.0	LWR11662-HI	0.138
	880.16681	100.0	SWP15155-LO	0.162
	880.48204	40.0	LWR11666-HI	0.321
	880.43312	100.0	SWP15159-LO	0.346
	881.15485	60.0	LWR11672-HI	0.660
	881.20675	80.0	SWP15165-LO	0.686
	881.51772	65.0	SWP15168-LO (d)	0.843
	881.56407	60.0	LWR11676-HI	0.866
	881.59343	15.0	SWP15168-LO (d)	0.881

Notes

(a): JD's and phases are given for mid-exposure; orbital phases are calculated according to the ephemerides in Table 1; (b): HI = High-dispersion; LO = Low-dispersion; (c): Flare spectra discussed by Linsky et al. (in preparation); (d): SWP15168 consisted of two separate exposure; these were summed for the purpose of this paper.

Spectra were obtained through the large aperture in both the short-wavelength range (SWP: 1150–2000 Å) at low dispersion and the long-wavelength region (LWR: 2000–3200 Å) at high dispersion (see Boggess et al., 1978 for instrumental details). A journal of the observations is given in Table 2. In this table four additional LWR and four SWP spectra of AR Lac, which were obtained by the Catania group in July 1979 and October 1980, are also included.

3. Results of simultaneous optical and UV observations

Our results are based on the output spectra produced by the standard processing software at both Vilspa and Goddard (Bohlin et al., 1981; Turnrose et al., 1982) and subsequent reduction with *IUEDR* processing software (Gidding, 1983). Line identifications were made by comparing a well-exposed spectrum of V711 Tau (SWP 15153) with the solar limb emission spectra published by Burton and Ridgeley (1970). In deciding which features in the solar limb spectrum might correspond to those in the stellar spectrum, the spectral resolution of *IUE* at low dispersion (~ 6 Å) and the relative intensities of the lines in Burton and Ridgeley's list were taken into account. The mean short wavelength spectra, with prominent emission lines identified, are presented in Fig. 2.

The SWP line fluxes were derived by numerically integrating the corresponding spectral features using a local background continuum defined on each side of a line. This approach seemed more satisfactory than applying an overall smoothed background. Integrated fluxes at Earth in the stronger lines were measured for each individual spectrum, and the results are presented in Tables 3 to 5. Most of the spectra were reduced independently at Armagh, Catania, and JILA, and there were only minor systematic differences – owing to different methods in defining the background continuum – in the results from the different institutions.

The Mg II k fluxes were determined for each stellar component using the high-dispersion LWR spectra. Multiple gaussian fits were applied to the observed profiles, allowing us to determine the flux of the K star, the G star, and the interstellar absorption in each image (Table 6). We will discuss this technique further in Sect. 4.

Integrated line fluxes extrapolated to the stellar surface, i.e. surface fluxes, can be computed with the conversion factors given in Tables 7 and 8 for each of the programme stars. The definition we adopted for these conversion factors deserves a few comments.

The conversion factor to compute surface fluxes (F) from observed fluxes (f) for a single star of radius R and distance d – is given by

$$F/f = (d/R)^2 = (2/\theta)^2, \quad (1)$$

where $\theta = 2R/d$ is the angular diameter in radians. If θ is given in milliarcsec and R and d are given in solar units and parsecs, respectively, Eq. (1) becomes

$$F/f = 1.966\,10^{15}(d/R)^2 = 1.702\,10^{17}\,\theta^{-2}. \quad (2)$$

The use of Eq. (2) requires knowledge of the distance and radius or an indirect determination of the angular diameter, for example from the improved Barnes-Evans empirical relation (Barnes et al., 1978), which involves only the intrinsic V_0 magnitude and the $(V-R)_0$ or $(R-I)_0$ colours,

$$\log\theta = 0.759 - 0.2V_0 + 0.641(V-R)_0, \quad (V-R)_0 > 0.80 \quad (3)$$

$$\log\theta = 0.855 - 0.2V_0 + 0.712(R-I)_0, \quad (R-I)_0 > 0.42. \quad (4)$$

The angular diameters θ (in milliarcsec) so derived offer the advantage of being independent of estimates of the star's radius and distance. However, they require accurate photometric data, which are not always available.

Since we are dealing with binary systems, an average conversion factor, which assumes equal surface flux on both stars, can be computed from the joint photometry. However, if the fractional contributions of each star ($\beta 1$ and $\beta 2$) to the total observed flux in a given line are known, it is possible to compute the surface flux for each star

$$F_1/f = 1.966\,10^{15}\,\beta_i(d/R_i)^2 = 1.702\,10^{17}\,\beta_i\theta_i^{-2}, \quad (5)$$

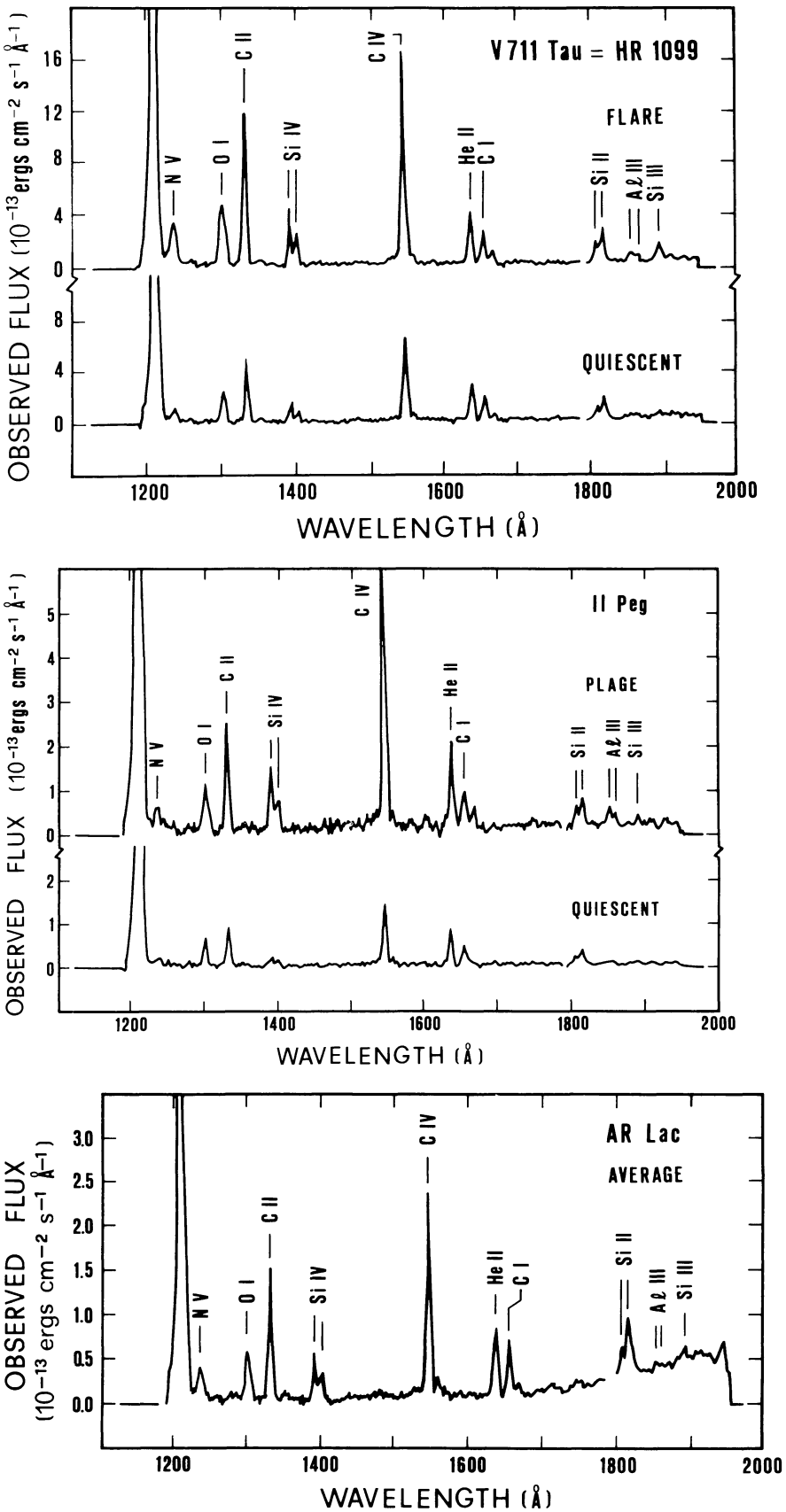

Fig. 2. Mean short wavelength spectra for V711 Tau during (a) flare and (b) quiescent, (c) II Peg active and (d) quiescent, and (e) AR Lac (average). The most prominent emission lines are identified

Table 3. Integrated line fluxes at Earth for V711 Tau from low-dispersion spectra obtained with *IUE* in units of 10^{-14} erg cm^{-2} s^{-1} a

	SWP:	15183	15158	15167	15170	15173	15197	15153		Average flux		
	Phase:	0.011	0.078	0.429	0.565	0.673	0.684	0.906		Present Paper	Linsky et al.	Simon & Linsky
Ion	(lambda)	(A)	(A)		(Q)	(Q)	(Q)	(A)	⟨A⟩/⟨Q⟩	(1981)	(1978)	(1980)
C III	(1175)	138	132	96	102	103	103	130	1.30	115±16	100	92
N V	(1240)	81	56	60	41	63	59	63	1.23	60±12	32	67
O I	(1304)	162	178	150	153	152	161	153	1.05	158± 9	138	-
C II	(1335)	286	330	256	234	252	228	273[b]	1.24	266±32	207	190
Si IV	(1394)	80	77	74	60	66	47	73	1.33	68±11	53	48
Si IV + O IV	(1402)	65	61	70	37	48	53	51	1.28	55±10	53	48
C IV	(1550)	396	438	412	328	354	329	408[b]	1.23	381±40	299	310
C I	(1561)	40	35	25	25	24	45	26	1.08	31± 8	-	-
He II	(1640)	160	172	167	152	146	164	157	1.06	160± 8	138	-
C I	(1658)	109	130	106	88	104	109	110	1.16	108±11	83	-
O III + Al II + Fe II	(1666)	50	44	37	38	30	30	42[c]	1.39	39± 7	19	-
Si II	(1808)	46	59	45	47	61	30	56	1.17	49±10	48	48
Si II	(1817)	101	117	90	98	109	94	111	1.09	103± 9	117	110
Al III + Fe III	(1855)	15	22	15	17	25	24	28	1.12	21± 5	36	-
Al III	(1862)	15	17	13	11	9	11	24		14± 5		
Si III	(1892)	30	28	31	30	32	23	34	1.08	30± 3	34	38
C III	(1909)	29	25	31	20	30	36	35	1.03	29± 5	39	35

Notes

(A): Active phase; (Q): Quiescent phase; (a): All fluxes less than 10^{-13} erg cm^{-2} s^{-1} are highly uncertain; (b): Lines whose fluxes are marked thus had at least one saturated pixel at line peak; (c) Data possibly affected by IUE hot spot pixels.

where $i = 1$ or 2. Equation (5) requires values for the distance and radius or for the V_0 magnitude and $(V-R)_0$ and $(R-I)_0$ colours for each star in the binary systems, which may be based upon the spectral class or derived by other indirect methods.

The conversion factors derived from the dimensions and distances for V711 Tau, II Peg, and AR Lac are presented in Table 7, and those derived from the Barnes-Evans relation are presented in Table 8. β_i values in these tables are derived from the Mg II lines and should only be applied with caution to SWP line fluxes. There is satisfactory agreement between the conversion factors derived by using the two methods in the case of V711 Tau. The discrepancy in the case of II Peg can be attributed to uncertainty in the distance to the star. Vogt (1981) suggested a large distance for II Peg and a radius of 2.2 $R_\odot$. The distance of 60–70 parsecs that is suggested by one low-weight parallax measurement (Jenkins, 1963) would imply a larger radius, and consequently the $v \sin i$ of 21 km s^{-1} (Vogt, 1981) would require a much larger inclination $60° < i < 90°$. This is consistent with the spot-plage scenario outlined above.

The integrated emission-line fluxes are plotted against orbital phase in Figs. 3 to 5 (bottom panel). The V magnitude light curves from ground-based observations (dots) and from two-spot modelling (broken curve) in Paper I are also given in the middle panel of these figures. The phase interval of visibility of each spot is shown in the upper panel of each figure. The orbital phases are calculated from the ephemerides in Table 1 for the time of mid-exposure of each spectrum.

The *IUE* Fine Error Sensor (FES) V band data showed broad agreement with the ground-based photometry (see Paper I), but the overall scatter was much greater than in the ground-based light curve. This scatter was expected from the precision of the FES itself. Therefore, the FES data were omitted from Figs. 3 to 5.

Three observations of V711 Tau from near phase 0.2 to 0.3, which were obtained during a large radio flare at JD 2444880.79 (P.A. Feldman and F. Roy, private communication), were high in a manner reminiscent of flaring. The fluxes measured for images SWP 15161 ($\phi = 0.183$), SWP 15163 ($\phi = 0.285$), and SWP 15164 ($\phi = 0.310$) are omitted from Table 3. These spectra show strong enhancement of all chromospheric and transition region lines with increasing flux ratio in passing from low to high temperature of formation. Another paper in this series

Table 4. Integrated line fluxes at Earth for II Peg from low-dispersion spectra obtained with *IUE* in units of 10^{-14} erg cm^{-2} s^{-1} a

	SWP:	15151	15160	15166	15171	15174	15182	15196	15147	Mean Quiet	Mean Active	
	Phase:	0.009	0.151	0.252	0.341	0.384	0.500	0.784	0.936	Hemisph	Hemisph	
Ion	(lambda)	(Q)	(Q)	(Q)	(Q)	Q)	(A)	(A)	(A)	<Q>	<A>	<A>/<Q>
C III	(1175)	16	23	46	30	36	122	52	127	30±10	100±34	3.3
N V	(1240)	11	9	10	12	5	28	39	31	9± 2	33±5	3.5
O I	(1304)	36	39	30	32	31	73	61	71	34± 3	68±5	2.0
C II	(1335)	41	42	41	52	38	140[b]	89	143[b]	43± 5	124±25	2.9
Si IV	(1394)	7	8	9	14	7	99	61	80	9± 3	80±16	8.9
Si IV + O IV	(1402)	6	7	10	5	8	54	41	41	7± 2	45± 6	6.3
C IV	(1550)	98	77	94	133	74	531[b]	326	454[b]	95±21	437±85	4.6
C I	(1561)	6	14	7	14	13	25	27	15	11± 4	22± 5	2.1
He II	(1640)	43	47	48	45	40	158	65	111	45± 3	111±38	2.5
C I	(1658)	35	28	31	25	29	75	65	53	30± 3	64± 9	2.2
O III + Al II + Fe II	(1666)	8	8	5	8	7	59	32	27	7± 1	39±14	5.5
Si II	(1808)	12	12	11	10	14	36	17	29	12± 1	27± 8	2.3
Si II	(1817)	22	23	20	22	20	65	34	46	21± 1	48±13	2.3
Al III + Fe III	(1855)	6	3	5	4	4	58	26	30	4± 1	38±14	8.6
Al III	(1862)	-	-	3	-	3	46	15	16	<3	26±14	>8.6
Si III	(1892)	4	3	5	6	5	24	7	18	5± 1	16± 7	3.5
C III	(1909)	8	6	5	6	4	22	10	7	6± 1	13± 6	2.2

Notes

(A): Active phase; (Q): Quiescent phase; (a): All fluxes less than 10^{-13} erg cm^{-2} s^{-1} are highly uncertain; (b): Lines whose fluxes are marked thus had at least one saturated pixel at line peak.

(Linsky et al., in preparation) will discuss these flare observations. A radio flare on II Peg, beginning about JD 2444879.62, might also have been recorded by these same observers, but no *IUE* spectra of II Peg were being taken at this time.

3.1. *V711 Tau (K1 IV + G5 V)*

The *V* light curve at the epoch of the *IUE* observations shows a fairly smooth variation with a total amplitude of $\Delta V \sim 0.1$ and a definite peak near phase 0.8 (Fig. 3, middle panel).

The two-spot model developed in Paper I assumes that the primary (i.e., the more massive) K1 subgiant is the active component and that the stellar rotation axis is perpendicular to the orbital plane. At the time of our *IUE* observations, the observed light curve can be reproduced by two major cool spotted areas ($T_{spot} = 3500$ K) having radii of 23° (spot no. 1) and 22° (spot no. 2), located at latitudes of +60° and +10° and crossing the central meridian at orbital phases 0.19 and 0.56, respectively. Since the inclination of the rotation axis is 33° (Paper I), the high-latitude spot will always be visible, while the low-latitude one will be visible, at least in part, in the phase interval 0.20 to 0.92. The southern limb of the equatorial spot will be visible, however, for a much shorter phase interval (0.36 – 0.76), while its northern limb will always be visible.

We have compared our line fluxes in Table 3 with those of Linsky et al. (1978), corrected for a calibration error (see Simon et al., 1980a; Simon and Linsky, 1980). Although agreement is generally good, there is a distinct tendency for the earlier fluxes to lie at the lower end of the range we observe. This is most marked in the higher excitation species, suggesting that the outer atmosphere of V711 Tau was in a higher overall state of activity in 1981 than in 1978 and 1979. The striking changes of the optical light curve during and especially after the time of our *IUE* observations also suggest that the photospheric spot activity in 1981–82 was highly variable and in a relatively high state at all phases. The high activity level of V711 Tau in 1981 is confirmed by the observation of a large flare that occurred in the phase interval 0.1 to 0.3 in coincidence with maximum spot visibility (Linsky et al., in preparation).

The detection of rotational modulation of line fluxes can be difficult, because it is likely that plage-like features are evenly distributed all over the stellar surface, particularly at high activity levels. Disregarding the flare data, Fig. 3 does not show any clear evidence of rotational modulation in the lines formed near

Table 5. Integrated line fluxes at Earth for AR Lac from low-dispersion SWP spectra obtained with *IUE* in units of 10^{-14} erg cm^{-2} s^{-1} a

	Year:	1979	1979	1980	1980	1981	1981	1981	1981	1979	1980	1980	1981
	Month:	July	July	Oct.	Oct.	Oct.	Oct.	Oct.	Oct.	July	June	Oct.	Oct.
	SWP:	5777	5810	10329	10352	15155	15159	15165	15168	5777 5810	9275	10329 10352	15155 15159 15165 15168
Ion (lambda)	Phase:	0.37	0.87	0.65	0.24	0.16	0.35	0.69	0.84	Average flux			
N V (1240)		35	52	18	18	25	24	24	18	44	(34)	18	22
O I (1304)		65	61	23	18	40	38	38	33	63	80	20	37
C II (1335)		82	82	38	31	81	81	73	64	82	85	34	75
Si IV (1394)		39	33	12	9	29	23	27	24	36	50	10	26
Si IV + O IV (1402)		27	44	11	9	18	18	20	17	36	34	10	18
C IV (1550)		220	245	77	58	158	139	136	121	232	120	68	139
C I (1561)		-	-	-	5	14	5	10	8	-	-	-	8
He II (1640)		68	73	23	23	53	52	45	43	70	56	23	48
C I (1658)		52	66	18	26	46	43	43	43	59	71	22	44
O III + Al II + Fe II (1666)		18	20	5	4	12	15	12	14	19	47	4	13
Si II (1808)		23	15	8	8	22	18	18	19	19	32	8	19
Si II (1817)		54	44	19	21	44	43	44	43	49	110	20	43
Al III + Fe III (1855)		7	-	6	-	12	10	9	6	7	-	6	9
Al III (1862)		-	-	-	-	6	6	5	3	-	-	-	5
Si III (1892)		19	16	6	6	16	15	19	19	18	27	6	17
C III (1909)		14	17	-	4	16	18	20	20	16	11	4	18

Notes (a): All fluxes less than 10^{-13} erg cm^{-2}s^{-1} are highly uncertain.

$\log T_e \sim 4$, such as Mg II, C I, and Si II. However, some variability seem to be present for the lines formed at higher temperatures (near $\log T_e \sim 5$). We compared the line fluxes in SWP spectra at orbital phases 0.011, 0.078, and 0.906 with those at phases 0.565, 0.673, and 0.684, representing conditions close to maximum and minimum spot visibility, respectively. A modest ~ 1.1 mean enhancement factor results for the cooler ions, while the mean enhancement factor for the hotter ions (C IV, Si IV, N V) is ~ 1.3. Thus it appears that when the more active spotted hemisphere of the K1 subgiant is facing the observer, the higher excitation ions are preferentially enhanced.

From the observed line fluxes (Tables 3 and 6), the corresponding surface fluxes can be obtained with the conversion factors given in Tables 7 and 8. Given the β values, based on Mg II, and the stellar radii in Table 7, the surface flux from the G dwarf is a factor of two higher than from the K subgiant. In deriving the conversion factors listed in Table 8, we used the joint magnitude and colour for V711 Tau from Paper I, $V = 5.85$, $(V - R) = 0.81$, and $(R - I) = 0.59$, and we assumed $\Delta V = +1.9$, $\Delta(V - R) = -0.21$ between the G and K star (Allen, 1973, Johnson, 1966).

3.2. *II Peg (K2 IV)*

Figure 4 shows that the V light curve for II Peg at the time of our *IUE* observations is asymmetric with a rise to maximum that is steeper than the subsequent fall. There is good overall agreement between the V light curves from *FES* and ground-based photometry. As with V711 Tau, there is considerable scatter in the FES data, however. The asymmetric V light curve suggests a spot distribution that is extended in longitude, with at least two centres of activity displaced from one another in stellar longitude and having different areas and/or contrast with the surrounding photosphere. The large amplitude in V suggests that much of one star's hemisphere was covered by spots. Figure 4 shows a dramatic anti-correlation between the chromospheric and transition region line fluxes and the photometric light curve.

Table 6. Mg II k line fluxes at Earth from high-dispersion spectra obtained with *IUE* in units of 10^{-12} erg cm^{-2} s^{-1}

Image No.	Orbital Phase	f_{obs}[a]	f_K	f_G	f_{plage}
		A) V 711 Tau			
11660	0.916	28.89	25.09	5.13	0.89
11665	0.066	26.34	24.53	4.77	1.48
11668[c]	0.204	40.01	37.43	4.59	1.60
11670[c]	0.265	37.23	34.99	5.67	1.88
11671[c]	0.303	36.38	33.02	5.69	1.13
11674	0.424	27.56	24.76	4.74	1.94
11679	0.557	28.01	25.75	4.51	2.00
11683	0.680	27.63	23.29	5.37	1.17
11691	0.005	28.04	26.69	5.02	1.56
11715	0.684	26.85	23.12	5.09	0.96
		B) II Peg			
11652	0.929	5.35	6.35	-	-
11655	0.002	4.03	5.01	-	-
11667	0.145	4.20	5.08	-	-
11673	0.244	4.07	4.79	-	-
11680	0.334	4.21	4.82	-	-
11684	0.391	4.41	5.60	-	-
11690	0.495	5.98	6.98	-	-
11714	0.780	6.66	7.81	-	-
		C) AR Lac			
5023	0.398	7.88	-	-	-
5059	0.902	8.00	-	-	-
9003	0.680	8.67	-	-	-
9010	0.269	7.57	-	-	-
11662	0.136	7.30	5.67	2.18	1.05
11666	0.321	7.73	5.92	2.21	1.00
11672	0.660	8.62	6.79	2.35	1.28
11676	0.866	7.37	5.76	2.00	0.78

Notes

(a): Total flux observed at Earth; (b): Flux corrected for absorption by the interstellar medium (IS); the IS flux is given by $f_{IS} = -(f_{obs} - f_K - f_G - f_{plage})$;

(c): Flare spectra discussed by Linsky et al. (in preparation)

At approximately the time of photometric minimum every line shows a marked degree of enhancement. The enhancement is unlikely to be a temporary, flare-like phenomenon, since it was observed over almost a complete rotation of the star, i.e., in spectra taken 5 days apart (SWP 15147 at phase 0.936 and SWP 15196 at phase 0.784). The enhanced flux lasts for an interval of 0.5–0.6 in phase and has a very sudden onset and decline over an interval of 0.1 in phase. If the inclination of the rotation axis is 35°, as assumed in Paper I, a surface feature that is visible for one half of the period and produces such a rapid onset and decline could be either a compact emitting region located on the equator or an extended region at a latitude of $-20°$ below the equator with a longitudinal extension of $\sim 40°$.

The spot models in Paper I assume an inclination of the rotation axis of either 35° or 60° (see Table 5 of Paper I). The model yields two spots ($T = 3300$ K) with central meridian passage at orbital phases of ~ 0.50 (for spot no. 2) and ~ 0.80 (for spot no. 1) and angular radii of 16° and 25°–30°. The spots cover about 2% and 5–7% of the entire stellar surface, respectively. These spots are always visible, except for their southern limbs, and they cross the stellar central meridian about 0.1 in phase earlier than the two major peaks on the light curves of the C IV, C II, and Si II lines. One possible interpretation of these peaks is that there are two major plages in the chromosphere and transition region of II Peg. However, a much simpler explanation is a single major equatorial plage, and the "peaks" are due to temporal changes.

Due to the uncertainty in the inclination of the rotation axis, we show in Fig. 1 spot solutions for both $i = 35°$ and $i = 90°$. The latter solution yields a large spot (no. 1) with a radius of 43° in the northern hemisphere, close to the position of spot no. 1 in the solution for $i = 35°$. Spot no. 2 in the $i = 35°$ solution is now split into two spots of nearly equal radii of 17° (no. 2) and 20° (no. 3), at latitudes of 0° and $-45°$, respectively. In the $i = 90°$ solution there is a close correlation between spot no. 2 and the enhanced line flux observed at phases 0.500, 0.784, and 0.936. If we attribute the enhanced line flux to a single equatorial plage, then the plage would be located at the trailing edge of spot no. 2 in the solution for $i = 90°$. Based on this interpretation, the other spots do not have such bright a plage associated with them, and the dip in the UV line flux at phase 0.784 indicates temporal variability.

The relatively quiescent portion of the flux curve is rather flat, indicating that the errors in our flux determinations are quite small. The "quiescent" phase interval from 0.0 to 0.4 yields mean fluxes and the associated rms errors, as given in Table 4. The larger error for C IV is almost entirely due to the high point at phase 0.341. Omitting this value reduces the scatter, giving mean value $86 \pm 11\ 10^{-13}$ erg cm^{-2} s^{-1}.

The degree of enhancement of each line in the plage depends on excitation temperature, i.e., lines of ions of higher excitation show greater enhancement. These enhancements range from 8.9 for Si IV, 6.3 for Si IV + O IV, and 4.6 for C IV to 2.3 for Si II and 2.0 for O I. This is similar to the effect noted in the case of V711 Tau and to an extent comparable to the enhancement observed during the flare on V711 Tau (Linsky et al., in preparation).

From the observed II Peg line fluxes in Tables 4 and 6, the corresponding surface fluxes can be obtained from the Barnes-Evans relation, as outlined in the previous section. The conversion factor is given in Table 8. Alternatively, we derived the conversion factor from Eq. 2 with $R = 2.3\,R_\odot$ and $d = 37$ parsecs (Table 7).

3.3. *AR Lac (G2 IV + KO IV)*

The optical light curve for AR Lac is complicated both by the fact that the system is eclipsing and by appreciable ellipticity and reflection effects (Chambliss, 1976). In order to concentrate on the intrinsic variations, the *V* light curve in Fig. 5 from Paper I omits the eclipses and has been corrected for the ellipticity effect, which would produce equal maxima at phases 0.25 and 0.75. From a Fourier analysis of the AR Lac light curve in Paper I, we derived a residual light variation due to spots with the deeper minimum near phase ~ 0.15, the maximum near ~ 0.80, and a peak-to-peak amplitude in *V* of ~ 0.05. The variation appears to be asymmetric, with a rise to maximum slower than the subsequent decline to minimum. The spot modelling in Paper I indicates that the residual light variation can be attributed to two cool spotted areas ($T \sim 3500$ K) on the K0 component each having 15° radius, located at a latitude of $+20°$ and $+50°$, and crossing the central meridian at phases ~ 0.21 and ~ 0.57, respectively (Fig. 1).

Table 7. Conversion factors (F/f) between surface flux (F) and observed flux (f) derived from stellar radius and distance

Star	Spectral Type	d (pc)	$R/R_\odot$	θ (milli-arcsec)	β_i[a]	F/f	Notes
V 711 Tau	K1 IV + G5 V	31	3.9 + 1.3	1.23	1.00	1.12×10^{17}	(c)
	K1 IV	31	3.9	1.17	0.83	1.03×10^{17}	(c)
	G5 V	31	1.3	0.39	0.17	1.90×10^{17}	(c)
II Peg	K2 IV + ?	30	2.8[d]	0.87	1.00	2.25×10^{17}	(b)
AR Lac	K0 IV + G2 IV-V	40	2.77 + 1.52	0.74	1.00	3.11×10^{17}	(b)
	K0 IV	40	2.77	0.64	0.73	3.03×10^{17}	(c)
	G2 IV-V	40	1.52	0.35	0.27	3.75×10^{17}	(c)

Notes

(a): β_i is the flux fraction due to the indicated component of the system for Mg II lines; (b): Mean conversion factor from Equation 2, assuming same surface flux for both stellar components; (c): Conversion factor for individual stellar components from Equation 5, assuming uniform brightness; (d): Lower limit from equating the stellar circumference with the product of equatorial velocity (v sin i = 21 km/s) and the rotational modulation period (6.72 days).

Table 8. Conversion factors (F/f) between surface flux (F) and observed flux (f) derived from photometric data

Star	Spectral Type	V_o	$(V-R)_o$	θ (milli-arcsec)	β_i	F/f[a]	$(R-I)_o$	θ (milli-arcsec)	F/f[a]
V 711 Tau	K1 IV + G5 V	5.85[b]	+0.81	1.28	1.00	1.04×10^{17}[c]	0.59	1.27	1.06×10^{17}[c]
	K1 IV	6.02[d]	+0.84[e]	1.24	0.82	0.91×10^{17}[f]	-[g]	-	-
	G5 V	7.92[h][d]	+0.63[e]	0.38	0.18	2.21×10^{17}[f]	-[g]	-	-
II Peg	K2 IV + ?	7.44[b]	+0.89	0.69	1.00	3.58×10^{17}[c]	0.72	0.76	2.95×10^{17}[c]

Notes

(a): β_i is the flux fraction in the Mg II lines due to the indicated component of the system; (b): Joint photometry of system component; (c): Mean conversion factor from Equation 2, assuming same surface flux for both components; (d): Assuming ΔV (G5-K1) = 1.9; (e): Assuming $\Delta(V-R)$ = -0.21; (f): Conversion factor for the individual components from Equation 5, assuming umiform brightness; (g): Magnitudes and colour data are not available; (h): Uncertain magnitude and colour affecting the derived conversion factors.

The small observed variation in V can be modelled by a low overall level of spottedness, spots evenly distributed in longitude, or by spots on the two stars on opposite hemispheres. This in turn would be consistent with the low level of contrast between the two hemispheres of AR Lac implied by the small variation of the UV line fluxes. Previous studies of the optical emission of AR Lac (Naftilan and Drake, 1977, and references therein) indicate that the K0 star has a higher chromospheric radiative loss rate. In the UV, Walter et al. (1983) and our Mg II data (see below) both suggest that the K0 star dominates the UV emission from the system. Nevertheless, the observed flux ratio of the K0 to the G2 star is slightly lower than the ratio of their surface areas ($\sim$3.3), and hence the G2 star has a slightly higher Mg II surface flux than the K0 star.

The line flux variations of AR Lac in the short-wavelength region show little evidence for changes that are correlated with the spot-induced optical variation. For the strongest line, C IV, minimum flux occurs near optical maximum at phase $\sim$0.80,

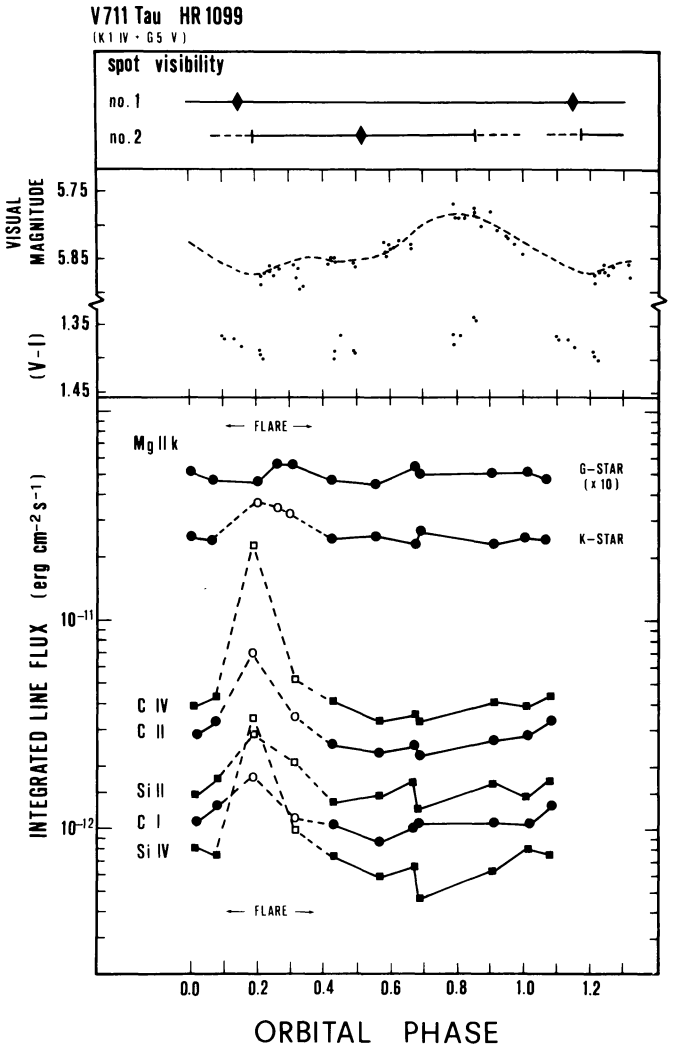

Fig. 3. *Upper panel:* phase intervals of spot center visibility (*continuous line*) for V711 Tau from models in Paper I; *full diamonds* mark the phases of spot center passage at stellar meridian; *broken lines* indicate the phase intervals during which the center of a partially visible spot is not on the visible hemisphere. *Middle panel:* ground-based photometry (*dots*) and mean light curve (*broken line*) from spot models in Paper I. *Bottom panel:* Line-flux as a function of orbital phase. Flare data (*open symbols*) are discussed by Linsky et al. (in preparation)

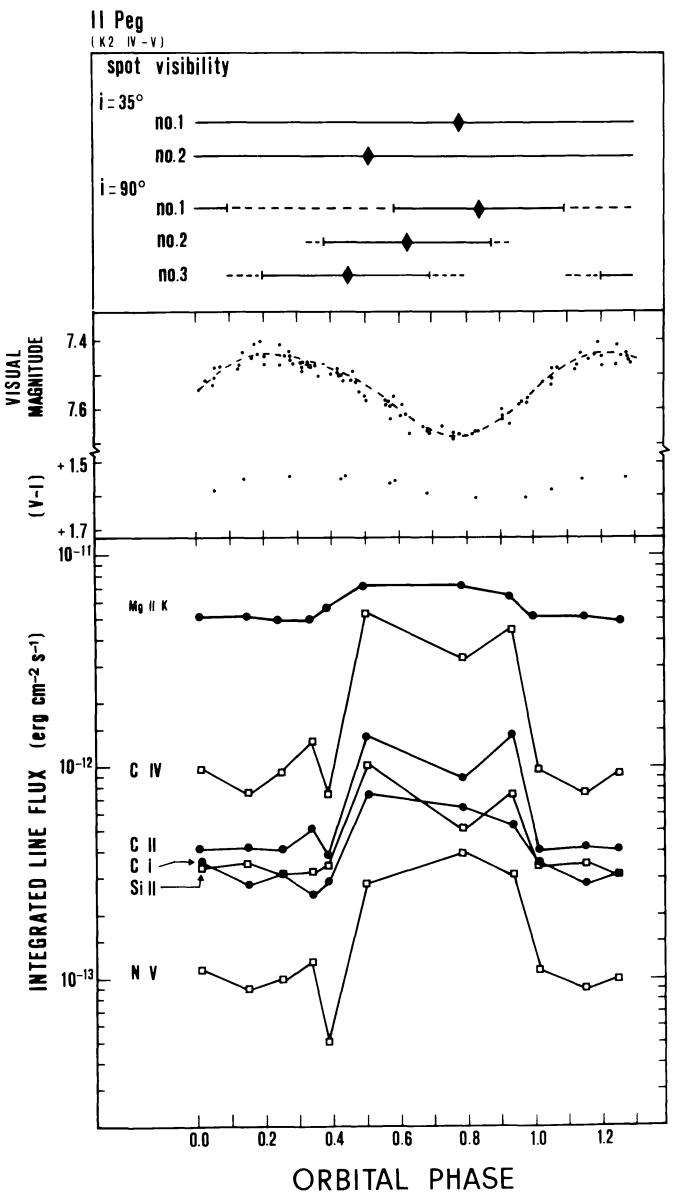

Fig. 4. As Fig. 3, but for II Peg

although the fainter lines in these weakly exposed low-dispersion spectra have a less clear-cut variation.

The G2 primary shows less than 10 percent variation of the Mg II k line flux versus phase. The K0 secondary, on the other hand, shows a definite variation of the Mg II k line flux with phase, which reaches a peak at phase 0.660. This is shortly after meridian passage of spot no. 1, suggesting that this spot is on the K0 secondary. The Mg II flux returns to its low level by phase 0.866. It should be noted that there is no Mg II flux increase at the time of meridian passage of spot no. 2, but maximum flux for the higher excitation lines, such as C IV and N V, is observed close to this phase, suggesting that spot no. 2 is on the G2 primary.

The association of line flux relative maxima with meridian passage of spots is consistent with the results for V711 Tau and II Peg. This trend suggests a spatial correlation between photospheric spots and plages in the outer atmosphere, as for the Sun.

Conversion factors to derive surface fluxes from those observed at Earth (Tables 5 and 6) are given in Table 7.

Our fluxes in 1981 are generally comparable with those of Walter et al. (1983), although the mean seasonal fluxes from July 1979 to October 1981, which are given in the last four columns in Table 5, clearly indicate some long term variability. It is interesting that between July 1979 and June 1980 the fluxes of high excitation lines, e.g., N V, C IV, and He II, decreased while those of the low excitation lines increased. The line fluxes are smallest in October 1980 and then appear higher again in October 1981.

4. High-resolution Mg II line profiles

Profiles of the Mg II h (λ 2802.7 Å) and k (λ 2795.5 Å) are plotted in Figs. 6 and 7 for V711 Tau and II Peg, respectively. The Mg II

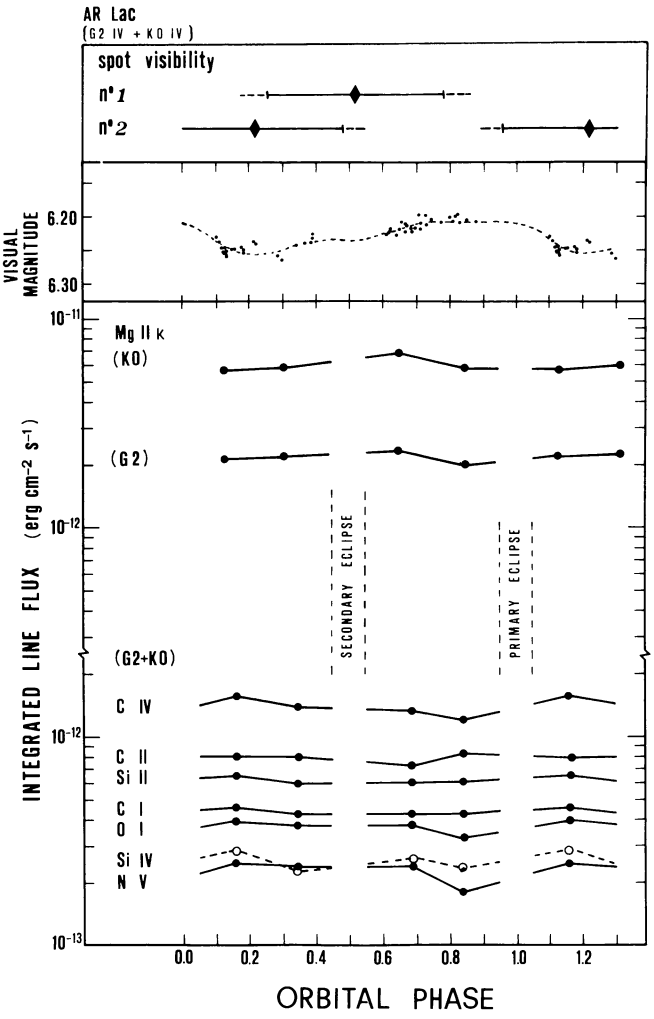

Fig. 5. As Fig. 3, but for AR Lac.

k line profiles for AR Lac are presented in Fig. 8. The wavelength scale is that produced by the IUEDR software (Gidding, 1983). All of the line profiles show a more or less prominent notch or narrow absorption feature at approximately a constant wavelength, which we interpret as the interstellar Mg II feature. A comparison of our spectra with the mean Mg II profiles of V711 Tau derived from *Copernicus* data by Anderson and Weiler (1978) suggests that this is an appropriate interpretation. In Figs. 6, 7 and 8 we have indicated the wavelength of the interstellar feature by vertical lines.

The Mg II k fluxes presented in Table 6 and Figs. 3–5 were determined by fitting a gaussian emission line to the global emission from each star and a gaussian absorption line of instrumental width to the interstellar feature. The measured wavelength of the interstellar feature was constant to an accuracy of about $\pm 3\,\mathrm{km\,s^{-1}}$, so it was subsequently used to calibrate the velocity scale. In a second round of fits we constrained the stellar emission profiles to be centered on their predicted positions. The resulting residuals can be interpreted as discrete emission components, and these will be discussed below. A more comprehensive discussion of the Doppler imaging technique of these spectra will be presented in later papers in this series (Walter et al., 1986). Since we are concerned only with the rotational modulation of the integrated stellar flux, we include the flux of these additional features in the total K star flux.

Two component gaussian fits of II Peg Mg II line profiles were made independently at Armagh, Catania and JILA to test the consistency of reduction methods. The three independent reductions give similar trends for the variation of the integrated line flux versus phase, although there are some systematic differences in the flux values, which may be due to different procedures in defining the faint continuum background. However, the discrepancies in absolute flux values are of the order of the expected photometric accuracy of *IUE*, ~15–20% (Cassatella et al., 1985). Internal accuracy is usually considerably better.

4.1. *V711 Tau*

Binary motion of the two emission components on V711 Tau is clearly seen against the center of mass wavelength. The radial velocities of the binary components were taken from the ephemeris of Fekel (1983) and are indicated in Fig. 6 by arrows. It appears from out data, however, that the larger K-star (shifted to the red in the phase interval 0.0–0.5) has the brighter Mg II features, a result in keeping with previous optical (cf. Fekel, 1983, and references therein) and UV measurements (Weiler et al., 1978; Simon and Linsky, 1980).

The Mg II k flux for each star of V711 Tau is shown in Fig. 3 (see also Table 6) as a function of orbital phase. Disregarding the flare (see Linsky et al., in preparation), both stars are constant, consistent with the lack of observed rotational modulation in the low-temperature SWP lines. The ratio of the observed Mg II flux in the two component stars is 4.7. However, the K star has 9 times the surface area of the G star, so the G star must have about twice the Mg II surface flux of the K star. If this ratio holds for the other lines, the surface fluxes for each star can be determined from the low-resolution SWP spectra (Tables 7 and 8).

The derived gaussian half widths (with the instrumental half-width removed) are $61 \pm 6\,\mathrm{km\,s^{-1}}$ for the K star and $47 \pm 2\,\mathrm{km\,s^{-1}}$ for the G star.

Residual emission could be seen in all spectra in excess of at least one of the K star gaussian wings. This emission could be due, at least in part, to a non-gaussian intrinsic profile. It might also be indicative of high-speed flows associated with active regions on the K star. Alternatively, it is possible to attribute the emission to two discrete plage regions in the atmosphere of the K star. Unfortunately, the blending of the K and G star profiles, coupled with the low signal-to-noise ratio in the line wings and the relatively poor phase coverage, it is difficult to distinguish among these possibilities. Later papers in this series will examine the behavior of these wings in more detail, making use of data obtained at several epochs.

Nevertheless, since we are concerned here only with rotational modulation of the component fluxes, and since the residual flux is included into total K star flux, the cause of the residual emission is unimportant in this context.

4.2. *II Peg*

Unlike V711 Tau, for II Peg there are no extant observations of interstellar absorption. Our Mg II spectra in Fig. 7 show a deep absorption feature, which appears at approximately the same wavelength at each orbital phase.

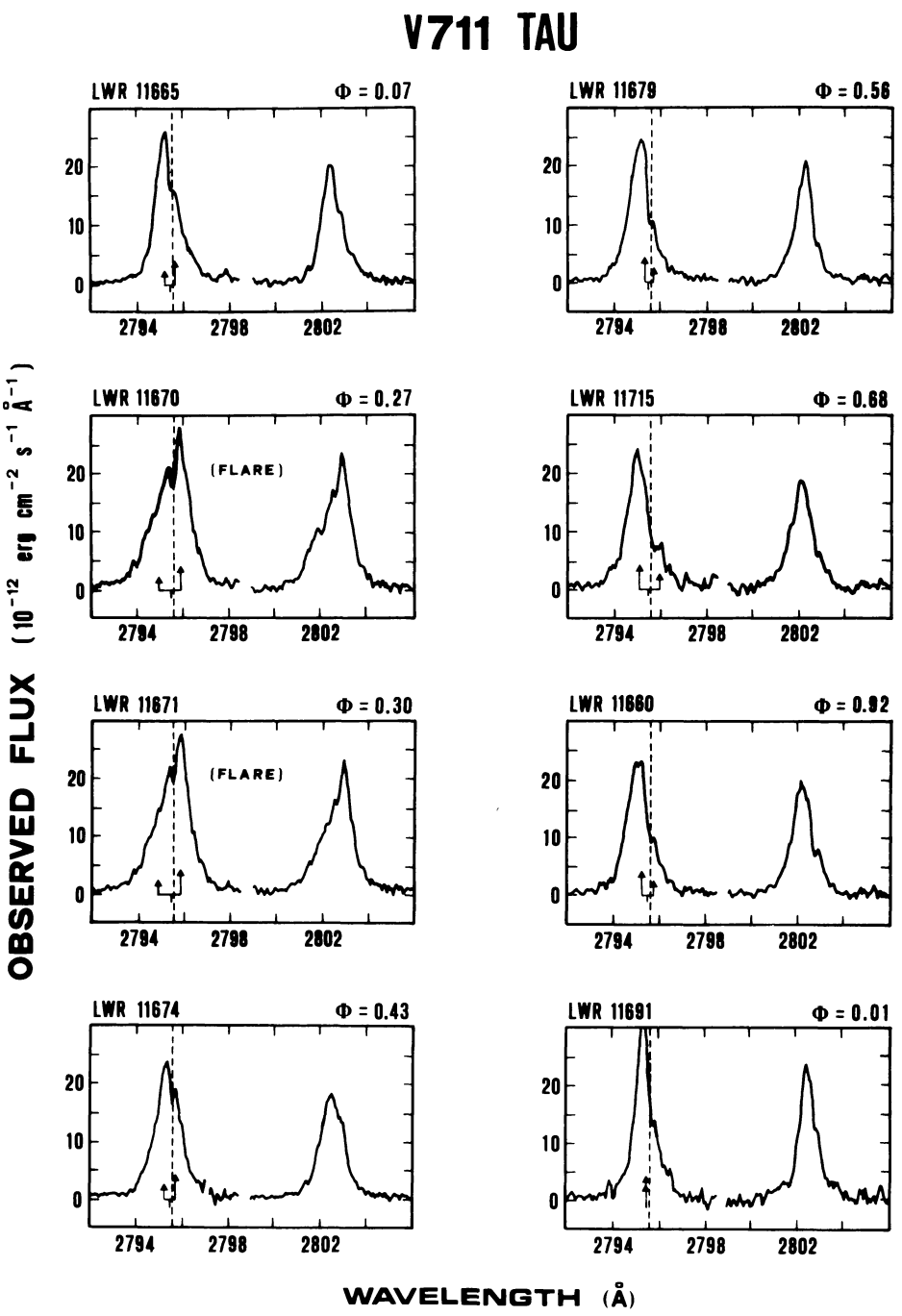

Fig. 6. Mg II h and k line profiles for V711 Tau at various orbital phases. *Broken vertical lines* indicate the interstellar Mg II wavelength according to Anderson and Weiler (1978). The interstellar wavelengths are ~0.2 Å redshifted with respect to the center of mass. The wavelengths of the expected emissions from the G5 and K1 stars are indicated by *arrows*. Longer arrows refer to the K-star. *Vertical downward marks* indicate the center of mass wavelength. The spectra LWR 11670 and LWR 11671 are affected by a large flare (see Fig. 3) and are discussed by Linsky et al. (in preparation)

The line profile fitting method also provides centroid wavelengths of the stellar and interstellar components. Their differences in radial velocity (all from data reduction at Armagh in order to ensure internal consistency) are plotted in the top panel of Fig. 9, where the mean radial velocity curve from Vogt's (1981) optical spectroscopy is drawn as a continuous line. The two radial velocity curves are quite similar, but Vogt's curve lies about $+5\,\mathrm{km\,s^{-1}}$ above our Mg II k-line curve. This is most likely due to a shift of the interstellar Mg II line relative to the velocity of the II Peg center of mass.

The line profile fits to the spectra near maximum radial velocity (LWR 11667, LWR 11673, and LWR 11714) show some evidence for emission from optically undetected faint secondary component of II Peg at an intensity level of ~5% with respect to the primary component. This suggestion is not conclusive, as similar bumps are seen on other spectra.

There is also evidence for high-velocity wings, as previously noted for V711 Tau. The wings are most prominent in the spectra taken at orbital phases 0.495 and 0.929, when the line fluxes are at a maximum. Since we are dealing with optically thick Mg II lines formed in a deep chromosphere, the broadening can be attributed, at least in part, to the increase of the line flux itself. To quantify this effect, theoretical profiles should be computed, but this is beyond the scope of the present paper. Both blue- and red-wings extend out to at least $+220\,\mathrm{km\,s^{-1}}$. The most extreme cases are the k line profiles at phases 0.495 (−165 and

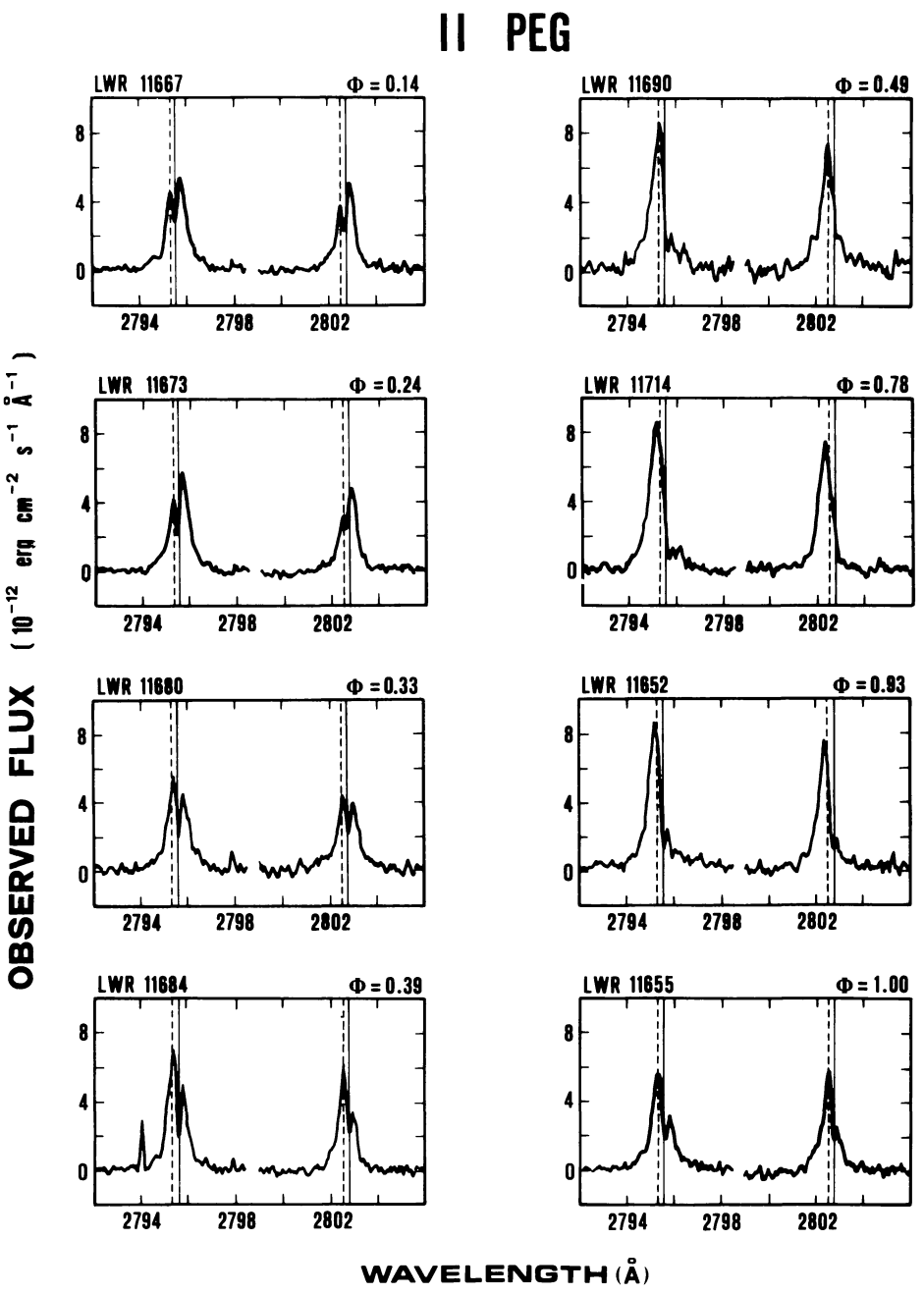

Fig. 7. Mg II h and k line profiles for II Peg as a function of orbital phase. *Broken vertical lines* indicate the center of mass wavelengths according to Vogt (1981). *Solid vertical lines* indicate interstellar Mg II absorption wavelength

$+220\,\mathrm{km\,s^{-1}}$) and 0.929 ($-200$ and $+275\,\mathrm{km\,s^{-1}}$). Our estimates of the extent of each line wing are plotted in the bottom panel of Fig. 10. We have averaged the measurements for the h and k lines; the errors indicate the difference between the individual values and the mean. These errors are consistent with the $\sim 20\,\mathrm{km\,s^{-1}}$ velocity resolution of *IUE* at 2800 Å. If these high velocity wings are real, then they could be explained by line-of-sight flow velocities along magnetic flux tubes associated with plages.

4.3. AR Lac

The Mg II k profiles for AR Lac are shown in Fig. 8. Also indicated are the wavelengths of the components of the binary, according to the orbital elements given by Sanford (1951). Some difficulty arises over which is the correct ephemeris to use. Evidence for changes in AR Lac's orbital period over the last eight decades have been discussed by Chambliss (1976) and Catalano (1983). For consistency we have used the ephemeris in Table 1 and in Paper I, which is based on contemporaneous photometry. Zero phase is defined by the center of the primary eclipse (the larger K0 star in front), so that any small difference with other authors should cause no difficulties here.

The arrows in Fig. 8 indicate the predicted positions of the line centers for each star at the time of each observation. The first notable feature of the profiles is that the emission from the K-star exceeds that from the G-star. This is consistent with previous optical (Sanford, 1951; Naftilan and Drake, 1977) and UV results (Walter et al., 1983).

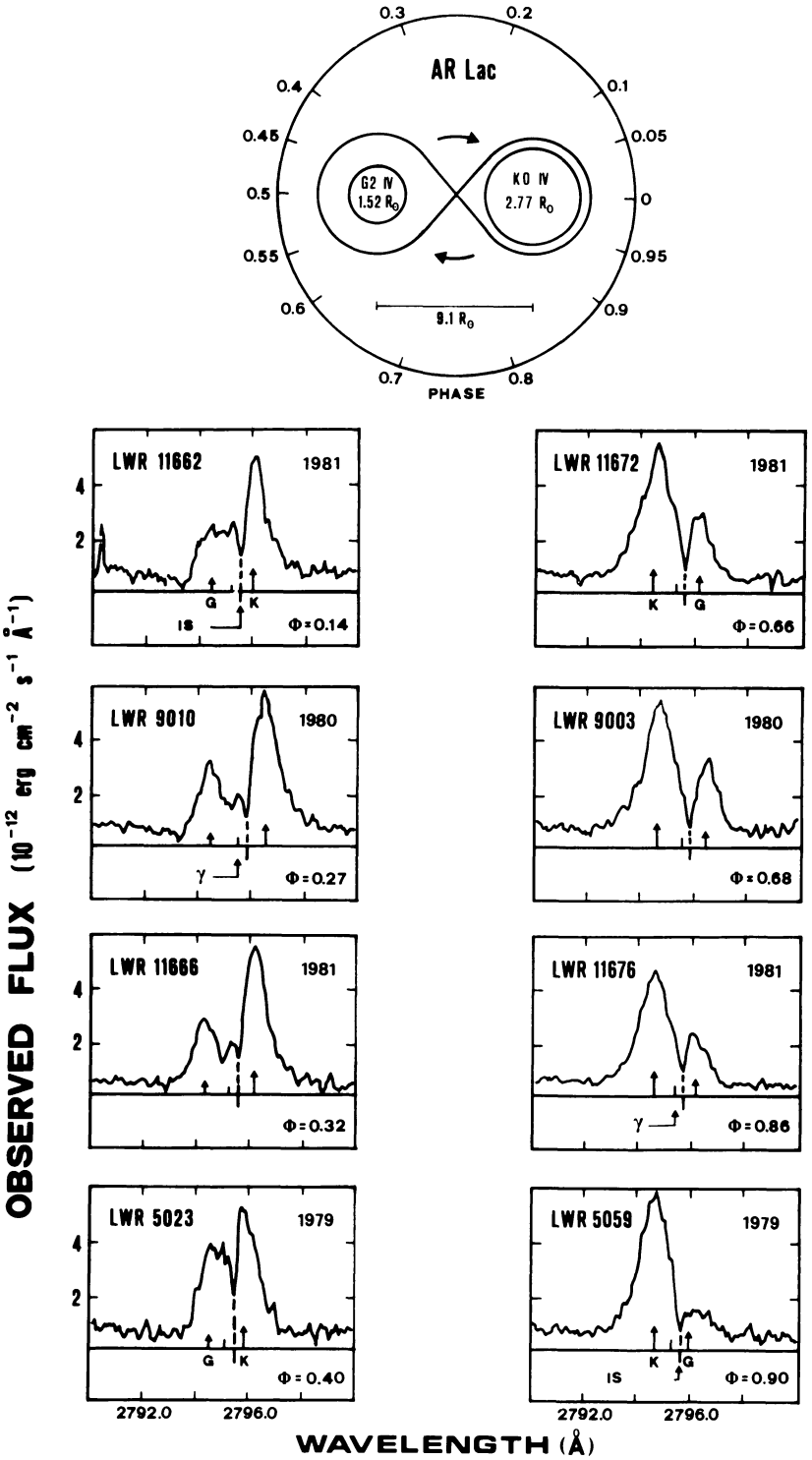

Fig. 8. Mg II k line profiles for AR Lac as a function of orbital phase. *Broken vertical lines* indicate the interstellar absorption wavelength (*IS*), while *arrows* indicate the expected wavelengths of the components of the binary from Sanford (1951). *Small upward marks* indicate the center of mass wavelength

We present our multiple gaussian fits to the Mg II k lines of AR Lac in Fig. 10. We attribute the two dominant emission features to uniform emission from the disk of the two stars. The absorption feature is of instrumental width and due to interstellar absorption. Residual emission is seen at all phases. We interpret this as emission from discrete regions on the K star, although other explanations are possible. A later paper in this series (Neff et al., in preparation) will discuss this emission in more detail, making use of spectra obtained at many epochs. In Table 6 we list the fluxes in these components. The K star fluxes in Table 6 and Fig. 5 include the excess emission.

The G star flux remained constant during the course of our observations. However, the K star flux increased at phase 0.660 by a factor of 1.2 compared to the mean flux defined by the other three spectra.

The lines due to the K star are broader than those of its companion. Sanford (1951) remarked on this phenomenon in the Ca II H and K lines. In Table 9 we list the measured line

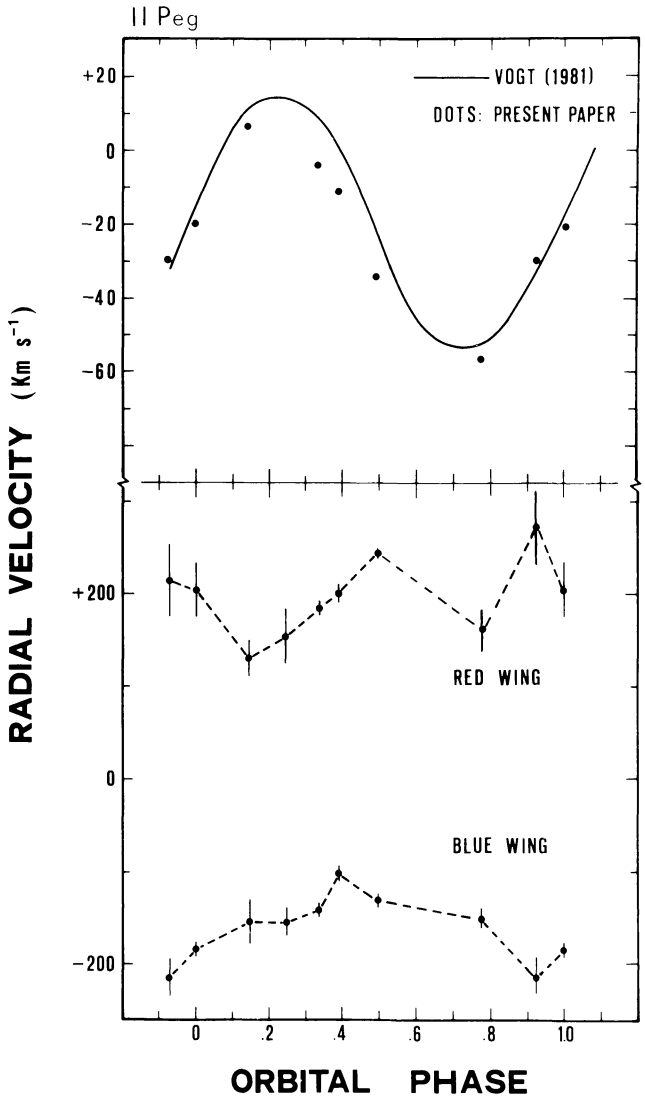

Fig. 9. *Upper panel:* radial velocity curve for II Peg obtained from radial velocity differences of the Mg II emission-line component relative to the superimposed interstellar absorption line (*dots*), and Vogt's (1981) mean curve from optical spectroscopy (*continuous line*). *Lower panel:* velocities of red and blue wings of the Mg II lines for II Peg. The plotted values are averages of the maximum velocity extent of h and k line wings

widths with the instrumental width removed. These values can be compared with what would be expected for a pair of uniformly emitting stars in synchronous rotation with the binary's orbital period of 1.983 days. The expected $v \sin i$ values of the K0- and G2-star for synchronous rotation are 72 km s^{-1} and 39 km s^{-1}, respectively, while the corresponding mean values in Table 9 are 72 ± 1 km s^{-1} and 61 ± 6 km s^{-1}.

Table 9. Deconvolved half-width (HWHM) of the Mg II h and k lines for AR Lac

LWR Image No.	Phase	HWHM (km s^{-1}) K-star	G-star
11662	0.136	72	66
11666	0.321	73	54
11672	0.660	73	57
11676	0.866	72	67

As with our results for V711 Tau and II Peg, we see excess emission in the line wings of AR Lac. In contrast with the other stars, however, this excess emission varies markedly with phase. We note that AR Lac has the highest $v \sin i$ of our program stars, which results in a broader observed profiles making it less likely to show weak line wings.

5. Conclusions

A common schematic model for all three stars incorporating a non-uniform brightness distribution extending from the photosphere to the transition region can account for the broad features of the observations presented above. By analogy with the Sun and, in particular, with solar active regions, we can describe a rough picture as follows.

The broad-band optical variations can be attributed to the existence of two large-scale spots or groups of spots that are unevenly distributed on the star's surface. As the star rotates, the varying aspect of the spots gives rise to broadband photometric variation. We presume that the localized occurrence of strong magnetic fields underlies the spot phenomenon, as in the case of the Sun. Where the magnetic fields extend into the outer atmospheres of the stars, they give rise to enhanced non-thermal energy deposition and resultant heating in plage-like features. The result of this is the observed variability with rotational phase of the high-temperature emission spectrum, which indicates chromospheric and transition region plages spatially associated with cool spots in the photosphere. In one case (II Peg) there is evidence that the plage is rather compact. These results deviate from a solar-type activity scenario in which plage area generally exceeds the surface area covered by spots. Evidence was also presented for long-term variability of AR Lac and for active surface features in both stellar components.

We see possible evidence for mass motions associated with these active areas. These could be due to flows, giving rise to excess emission in the wings and leading to apparent line broadening or asymmetries. An alternative explanation for the broadening at the base of the emission features in the Mg II lines is van der Waals collisional broadening, which would be largest in high density active regions. In the case of solar active regions the magnetic fields are organized into loop structures extending into the corona. It seems reasonable that similar structures form in the RS CVn star coronae, as suggested by Simon et al. (1980b) and Uchida and Sakurai (1983). The excess broadening that may be present in the II Peg Mg II lines at phases 0.495 and 0.929, when the plage apparently associated with spot no. 2 is at the stellar limb, could be due to flows along such loop structures. There is evidence, however, for discrete features in the line profiles of AR Lac.

In conclusion, we have presented strong evidence in favor for the existence of solar-like active areas in the atmospheres of late-type stars and for their association with dark spots that are presumably magnetic in origin. The surprisingly low or null rotational modulation of the observed flux in some lines for V711 Tau and AR Lac is likely due to the high activity level on these stars in the period of our *IUE* observations. Later papers in this series will discuss physical models.

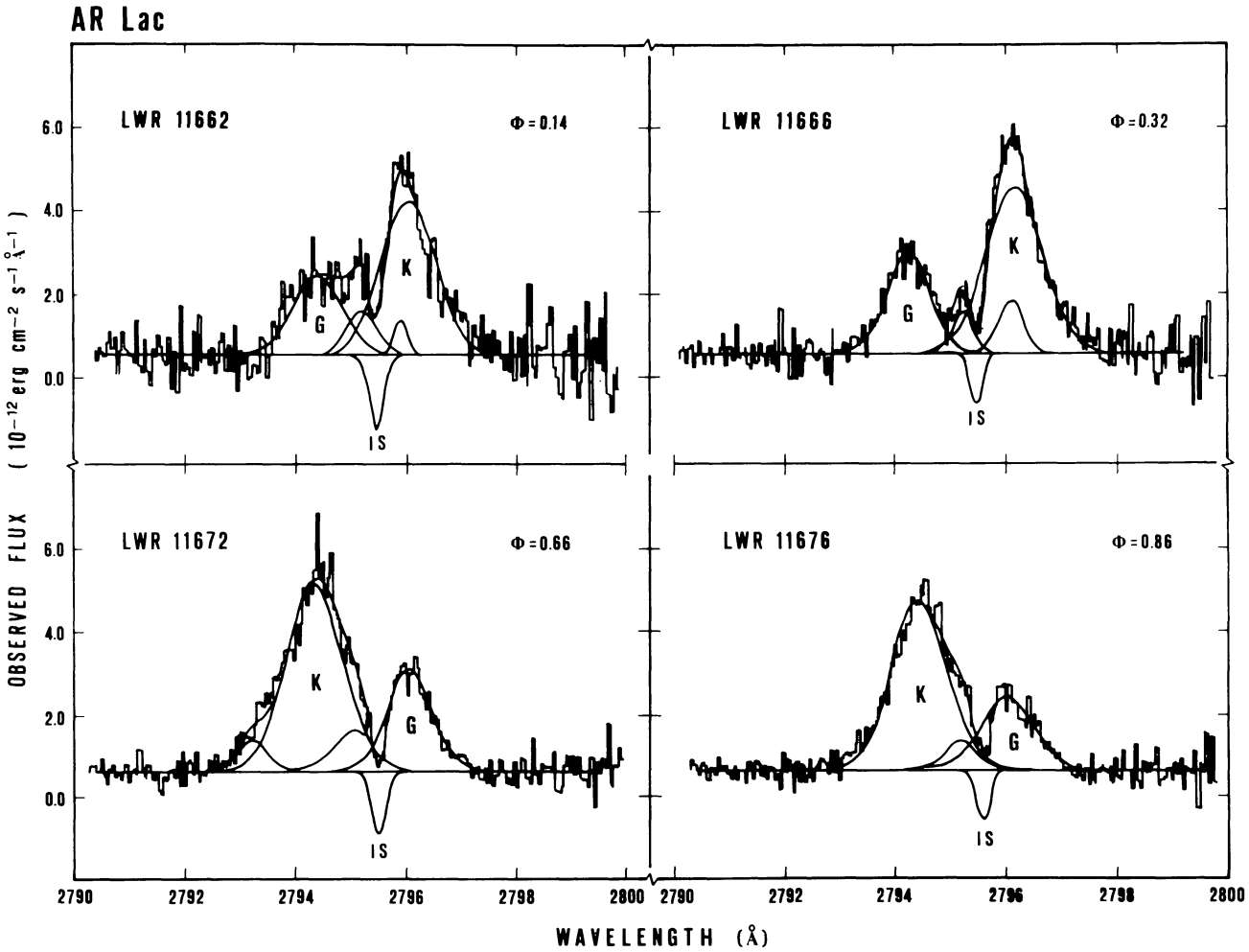

Fig. 10. Multiple gaussian fits to the Mg II k lines of AR Lac. The two dominant emission features are due to the K and G stars. The feature marked *IS* is due to interstellar absorption. Residual emission can be attributed to discrete features on the K star. Note the discrete feature is always close to the system γ velocity

Acknowledgements. We acknowledge support by several grants including NASA grant NAG5-82 to the University of Colorado, CNR-GNA grant to the Catania Astrophysical Observatory, CNR-PSN and "Ministero della Pubblica Istruzione" grants to the Astronomy Institute of Catania University, and a travel grant (no. 386/84) from the NATO Scientific Affairs Division to maintain the collaboration between Armagh, Boulder and Catania groups.

The data analysis was carried out at the Colorado Regional Data Analysis Facility, which is supported by NASA grant NAG5-26409 to the University of Colorado, at the Catania ASTRONET node, and at Armagh Observatory STARLINK terminal.

We wish to thank the three agencies ESA, NASA, and SERC for the allocation of time on *IUE* and their staffs for valuable help in the collection of data.

References

Allen, C.W.: 1973, *Astrophysical Quantities*, The Athlone Press, London

Anderson, R.C., Weiler, E.J.: 1978, *Astrophys. J.* **224**, 143

Andrews, A.D., Byrne, P.B., Butler, C.J., Linsky, J.L., Simon, T., Marstad, N., Rodonò, M., Blanco, C., Catalano, S., Marilli, E., Pazzani, V.: 1983, in *Activity in Red Dwarf Stars, IAU Coll.* 71, eds. P.B. Byrne, M. Rodonò, Reidel, Dordrecht, p. 443

Baliunas, S.L., Dupree, A.K.: 1982, *Astrophys. J.* **252**, 668

Barnes, T.G., Evans, D.S., Moffett, T.J.: 1978, *Monthly Notices Roy. Astron. Soc.* **183**, 285

Belvedere, G.: 1983, in *Activity in Red Dwarf Stars, IAU Coll.* 71, eds. P.B. Byrne, M. Rodonò, Reidel, Dordrecht, p. 579

Blanco, C., Catalano, S., Marilli, E.: 1979, *Nature* **280**, 661

Boggess, A., et al.: 1978, *Nature* **275**, 372

Bohlin, R.C., Holm, A.V., Lindler, D.J.: 1981, *IUE ESA Newsletter*, No. **10**, p. 10

Bopp, B.W.: 1983, in *Activity in Red Dwarf Stars, IAU Coll.* **71**, eds. P.B. Byrne, M. Rodonò, Reidel, Dordrecht, p. 363

Burton, W.M., Ridgeley, A.: 1970, *Solar Phys.* **14**, 3

Byrne, P.B., Butler, C.J., Andrews, A.D., Linsky, J.L., Simon, T., Marstad, N., Rodonò, M., Blanco, C., Catalano, S., Marilli, E.: 1982, *Third European IUE Conference*, ESA SP-176, p. 125

Byrne, P.B., Doyle, J.G., Andrews, A.D., Butler, C.J., Marstad, N., Linsky, J.L., Simon, T., Rodonò, M., Catalano, S., Blanco,

C., Marilli, E., Pazzani, V.: 1984, *Fourth European IUE Conference*, ESA SP-218, p. 343
Cassatella, A., Barbero, J., Benvenuti, P.: 1985, *Astron. Astrophys.* **144**, 335
Catalano, S.: 1983, in *Activity in Red Dwarf Stars, IAU Coll.* **71**, eds. P.B. Byrne, M. Rodonò, Reidel, Dordrecht, p. 343
Catalano, S.: 1986, in *Flares: Solar and Stellar*, ed. P.M. Gondhalekar, RAL Workshop 86-085, p. 105
Catalano, S., Rodonò, M.: 1967, *Mem. Soc. Astron. Ital.* **38**, 395
Chambliss, C.R.: 1976, *Publ. Astron. Soc. Pacific* **88**, 762
Charles, P.A.: 1983, in *Activity in Red Dwarf Stars, IAU Coll.* **71**, eds. P.B. Byrne, M. Rodonò, Reidel, Dordrecht, p. 415
Eaton, J.A., Hall, D.S.: 1979, *Astrophys. J.* **227**, 907
Fekel, F.C.: 1983, *Astrophys. J.* **268**, 274
Feldmann, P.A., Tayler, A.R., Gregory, P.C., Seaquist, E.R., Balonek, T.J., Cohen, N.L.: 1978, *Astron. J.* **83**, 1471
Gidding, J.R.: 1983, *IUE Newsletters* No. **17**, 53
Hall, D.S.: 1976, in *Multiple Periodic Variable Stars, IAU Coll.* **29**, ed. W.S. Fitch, Reidel, Dordrecht, p. 287
Hall, D.S.: 1981, in *Solar Phenomena in Stars and Stellar Systems*, eds. R.M. Bonnet, A.K. Dupree, Reidel, Dordrecht, p. 431
Jenkins, L.F.: 1963, *General Catalogue of Trigonometric Stellar Parallaxes*, Yale Univ. Obs.
Johnson, H.L.: 1966, *Ann. Rev. Astron. Astrophys.* **4**, 193
Linsky, J.L.: 1983, in *Activity in Red Dwarf Stars, IAU Coll.* **71**, eds. P.B. Byrne, M. Rodonò, Reidel, Dordrecht, p. 39
Linsky, J.L.: 1984, in *Cool Stars, Stellar Systems, and the Sun*, eds. S.L. Baliunas, L. Hartmann, Springer-Verlag, Berlin, p. 244
Linsky, J.L., Ayres, T.R., Basri, G.S., Morrison, N.D., Schiffer III, F.H., Holm, A., Cassatella, A., Heck, A., Macchetto, F., Stickland, D., Wilson, R., Blanco, C., Dupree, A.K., Jordan, C., Wing, R.F.: 1978, *Nature* **275**, 389
Marstad, N., Linsky, J.L., Simon, T., Rodonò, M., Blanco, C., Catalano, S., Marilli, E., Andrews, A.D., Butler, C.J., Byrne, P.B.: 1982, *Advances in Ultraviolet Astronomy, Four Years of IUE Research*, NASA-CP 2238, p. 554
Naftilan, S.A., Drake, S.A.: 1977, *Astrophys. J.* **216**, 508
Poe, C.H., Eaton, J.A.: 1985, *Astrophys. J.* **289**, 644
Rodonò, M.: 1981, in *Photometric and Spectroscopic Binary Systems*, eds. E.B. Carling, Z. Kopal, Reidel, Dordrecht, p. 283
Rodonò, M.: 1983, in *Achievements in Space Astrophysics*, eds. H.S. Hudson, A.K. Dupree, J.L. Linsky, *Adv. Space Res.* **2**, 225
Rodonò, M.: 1984, in *Space Research Prospects in Stellar Activity and Variability*, eds. A. Mangeney, F. Praderie, Obs. Paris-Meudon Press, p. 227
Rodonò, M.: 1986, in *Highlights of Astronomy*, ed. J.P. Swings, Reidel, Dordrecht, p. 429
Rodonò, M., Romeo, G., Strazzulla, G.: 1980, *Second European IUE Conference*, ESA SP-157, p. 55
Rodonò, M., Cutispoto, G., Pazzani, V., Catalano, S., Byrne, P.B., Doyle, J.G., Butler, C.J., Andrews, A.D., Blanco, C., Marilli, E., Linsky, J.L., Scaltriti, F., Busso, M., Cellino, A., Hopkins, J.L., Okazaki, A., Hayashi, S.S., Zeilik, M., Helston, R., Henson, G., Smith, P., Simon, T.: 1986, *Astron. Astrophys.* **165**, 135
Sanford, R.F.: 1951, *Astrophys. J.* **113**, 299
Simon, T., Kelch, W.L., Linsky, J.L.: 1980a, *Astrophys. J.* **237**, 72
Simon, T., Linsky, J.L.: 1980, *Astrophys. J.* **241**, 759
Simon, T., Linsky, J.L., Schiffer, F.M. III: 1980b, *Astrophys. J.* **239**, 911
Turnrose, B., Thompson, R., Bohlin, R.: 1982, *IUE ESA Newsletter* **13**, 8
Uchida, Y., Sakurai, T.: 1983, in *Activity in Red Dwarf Stars, IAU Coll.* **71**, eds. P.B. Byrne, M. Rodonò, Reidel, Dordrecht, p. 629
Vogt, S.S.: 1981, *Astrophys. J.* **247**, 975
Walter, F.M., Gibson, D.M., Basri, G.S.: 1983, *Astrophys. J.* **267**, 665
Walter, F.M., Neff, J.E., Gibson, D.M., Linsky, J.L., Rodonò, M., Gary, D.E., Butler, C.J.: 1986, *Astron. Astrophys.* (submitted)
Weiler, E.J., Owen, F.N., Bopp, B.W., Schmidtz, M., Hall, D.S., Fraquelli, D.A., Piirola, V., Ryle, M., Gibson, D.M.: 1978, *Astrophys. J.* **225**, 919